Contrib Mineral Petrol (2000) 139: 555–569

G. D. H. Simpson · A. B. Thompson · J. A. D. Connolly

Phase relations, singularities and thermobarometry of metamorphic assemblages containing phengite, chlorite, biotite, K-feldspar, quartz and H_2O

Received: 15 November 1999 / Accepted: 3 April 2000

Abstract The phase relations of divariant and trivariant assemblages involving combinations of phengite, chlorite, biotite, K-feldspar, quartz and H_2O in the KFASH, KMASH and KFMASH systems were calculated using a single thermodynamic data set (Holland and Powell 1998). The stability fields of the various equilibria are represented in *P-T* projections by contouring sets of compositional isopleths for the Tschermak ($Al_2(Fe,Mg)_{-1}Si_{-1}$) and $FeMg_{-1}$ exchanges controlled by the coexisting phases. Five multivariant continuous equilibria, which occur in different regions of *P-T-X* space, are calibrated as thermobarometers in metamorphic rocks of pelitic to quartzofeldspathic composition. More subtle *P-T* information, relating to the trajectories (dT/dz) along which reacting rocks have been buried or exhumed, can be extracted from the continuous reactions by investigating the recorded compositional trends in the $Al_2(Fe,Mg)_{-1}Si_{-1}$ and $FeMg_{-1}$ solutions. Singularities in *P-T* space are associated with some of these reactions and may result in unusual mineral textures and compositional trends. A fluid-absent singularity has particular petrological significance because it marks the transition between hydration and dehydration along a single reaction with increasing pressure and temperature. This behaviour causes the sequence of reactions among these minerals observed during metamorphism to be critically dependent on the *P-T* trajectory. Thermobarometric calculations show good agreement with respect to experimental and field-based data for phengite compositions less than about 50 mol% celadonite ($<\sim$3.5 Si p.f.u. phengite).

G. D. H. Simpson (✉) · A. B. Thompson · J. A. D. Connolly
Institut für Mineralogie und Petrographie,
ETH Zurich, Sonneggstr. 5, CH-8092, Switzerland

Present Address:
G. D. H. Simpson
Departement TAO, Ecole Normale Supérieure,
24 rue Lhomond, F-75231 Paris Cedex 05, France
E-mail: simpson@geologie.ens.fr

Editorial responsibility: W. Schreyer

1 Introduction

Low and medium grade metamorphic terrains contain abundant rocks of sedimentary and/or granitic origin. Although the assemblages of such rocks show relatively few changes in major mineralogy with pressure and temperature, it is possible to define their progressive metamorphism in terms of continuous reactions involving changes in the compositions of coexisting mineral phases along both Tschermak [$Al_2(Fe,Mg)_{-1}Si_{-1}$] and $FeMg_{-1}$ exchanges (J. B. Thompson 1957; A. B. Thompson 1976, 1982; Goffé 1977; J. B. Thompson 1979; Miyashiro and Shido 1985; Essene 1989; Spear 1989). In order to obtain information on the pressure and temperature history of rocks from sequences containing metamorphosed sediments and granites, it is necessary to have a quantitative understanding of the multivariant reactions existing between the phases phengite, chlorite, biotite, K-feldspar and quartz. This paper presents an investigation of these various reactions appropriate to metamorphism of pelitic and greywacke metasediments, felsic magmatic rocks and intensely weathered Al-rich rocks such as laterites.

Numerous workers have observed increases in the silica per formula unit (Si p.f.u.) in natural phengite with increasing pressure and decreasing temperature (e.g. Ernst 1963; Sassi 1972; Guidotti 1978, 1984). This is an observation confirmed and quantified experimentally for some reactions in the KMASH (K_2O + MgO + Al_2O_3 + SiO_2 + H_2O) system (phengite + biotite + K-feldspar + quartz + H_2O, Velde 1965; Massonne and Schreyer 1987; phengite + pyrope + kyanite + quartz + H_2O, Massonne and Szpurka 1997; phengite + talc + quartz/coesite + K-feldspar + kyanite + H_2O, Massonne and Schreyer 1989) and in the KFASH (K_2O + FeO + Al_2O_3 + SiO_2 + H_2O) system (phengite + almandine + kyanite + quartz + H_2O, Massonne and Szpurka 1997; see also Monier and Robert 1986). Following from these investigations, several workers have derived thermodynamic

data for the phengite end-members $KMgAlSi_4O_{10}(OH)_2$ (Mg-celadonite, Bucher-Nurminen 1987; Holland and Powell 1990, 1998; Powell and Evans 1983) and $KFeAlSi_4O_{10}(OH)_2$ (Fe-celadonite, Massonne and Szpurka 1997; Holland and Powell 1998). The extraction of these phengite data, along with thermodynamic data for the biotite and chlorite Tschermak free (Fe and Mg) end-members, has enabled calculation of compositional isopleths as a function of P-T-a_{H_2O} of a large number of previously uncalibrated equilibria (see: Bucher-Nurminen 1987; Powell and Holland 1990; Roots 1995; Worley and Powell 1998; Powell et al. 1998). These calculations are used extensively to constrain the pressure and temperature conditions for the equilibration of multivariant natural assemblages (e.g. Linner 1996; DiVincenzo et al. 1997; Goscombe et al. 1998; Graessner and Schenk 1999).

In the combined KFMASH system, there are one divariant equilibrium and six trivariant equilibria involving the six phases phengite, chlorite, biotite, K-feldspar, quartz and H_2O. Only one of these reactions has been considered experimentally (phengite + K-feldspar + biotite + quartz + H_2O, Massonne and Schreyer 1987). Investigations of natural parageneses have shown that microcline appears to be stable with chlorite at low metamorphic grade, whereas phengitic muscovite is stable with biotite at higher grades. Mather (1970) and Wang et al. (1986) have noted that K-feldspar and chlorite in metagreywackes give way to less phengitic muscovite and biotite at higher grade (see also: James 1955; Zen 1960; Graessner and Schenk 1999). The compositional variability and pressure-temperature (P-T) location of the various multivariant reactions involving chlorite and K-feldspar remain largely unknown. As with their higher grade counterparts, these low grade reactions can potentially be applied as continuous reaction thermobarometers.

In this paper we examine phase relations of multivariant equilibria existing among combinations of the phases phengite, chlorite, biotite, K-feldspar, quartz (and H_2O) in the KFASH, KMASH and KFMASH model systems with calculations performed using one thermodynamic data set (that of Holland and Powell, 1998). The principle aim of this paper is to quantify and understand the mineralogical changes and chemical exchanges that are recorded in natural assemblages as metamorphic rocks of sedimentary or granitic origin are buried and/or exhumed along particular P-T paths. This is achieved by calculating the positions of, and relationships among, various phase fields. The schematic relative topology of these has been considered previously (Bucher-Nurminen 1987; Wang et al. 1986). We wish to determine how well the various experimental and thermodynamic studies in model systems can be applied to natural occurrences for the purposes of thermobarometry, and to understand how existing thermodynamic data for common phyllosilicate phases can be extended to more complex natural systems.

As a result of the recent work to estimate thermodynamic data for Fe and Mg end-members for the common phyllosilicate phases (e.g. Massonne and Szpurka 1997; Holland and Powell 1998), petrologists are confronted with a variety of thermodynamic data. In our consideration of low grade metamorphism we have found that the results of calculations vary considerably with respect to the version of thermodynamic data set used (see Appendix). We have chosen here not to evaluate the various merits or limitations of particular data sets, but rather to use the data set of Holland and Powell (1998) to illustrate the natural reactions and to discuss the applications of our observations to understanding the metamorphic histories revealed by such rocks.

2 Calculated phase relations of phyllosilicate-bearing equilibria in model systems for low grade metamorphism

Thermodynamic calculations were performed with THERMOCALC (Powell and Holland 1988) using the solution models (Table 1) and internally consistent data set (Table A1) of version 2.5 (which was generated on 26 September, 1997). Biotite and chlorite were modelled using site populations and excess terms as in Holland and Powell (1998) and Holland et al. (1998). Calculations were also performed (though not presented here) using more recent chlorite and biotite models and data from Holland et al. (1998) and Holland and Powell (1999), but the results of these calculations are very similar to those presented here. The exception occurs at compositions very close to clinochlore at low temperatures where chlorites that are Al-deficient relative to clinochlore stoichiometry become stabilised (Holland and Powell 1999). We present the results in terms of conventional model systems (KFASH, KMASH and KFMASH) as a background to our petrological discussions. We do not consider here phases such as garnet and stilpnomelane, which may also be relevant to rocks of such composition at the metamorphic grade of interest (as discussed by Massonne and Szpurka, 1997). Throughout the text (see also Table 1), phases are denoted with three upper case characters whereas components are denoted with two lower case characters [as is the Tschermak vector, tk, $Al_2(Fe,Mg)_{-1}Si_{-1}$].

2.1 Choice of additive components for continuous reactions involving coupled substitutions

In our case, there are several advantages in choosing muscovite [ms, $KAl_2(AlSi_3)O_{10}(OH)_2$] rather than celadonite [ce, $K(Fe,Mg)Al(Si_4)O_{10}(OH)_2$] as the additive component for white mica. The most prominent advantage is that the KMASH or KFASH continuous reactions among phengite (PHE), biotite (BIO), chlorite (CHL), K-feldspar (KSP), quartz (QTZ), H_2O and Tschermak [tk, $Al_2(Fe,Mg)_{-1}Si_{-1}$] can be written as:

Table 1 Phase and component notation, site mixing models and activity-composition relations used in calculations (after: Holland and Powell 1998, 1999; Holland et al. 1998). The M2 site involved in mixing is bound by rounded-brackets, the M1 site is bound by cusp-brackets and the T2 site is bound by square-brackets. X_{Fe} is defined as Fe/(Fe + Mg), Y is defined as the proportion of Tschermak substitution (muscovite, $Y = X_{Al}^{M2}$; biotite, $Y = X_{Al}^{M1}$; chlorite, $Y = X_{Al}^{T2}$) and N is defined as $X_{Al,M2} - X_{Al,T2}$. Non-ideal (symmetrical) mixing is treated with the interaction parameters $W_{ms-ce} = 0$, $W_{am-cl} = 18$, $W_{cl-da} = 2.5$, $W_{am-da} = 20.5$, $W_{Al_2-Si(Fe,Mg)} = 10$, $W_{Mg-Fe} = 3$, (kJ). In this table and throughout the text, phases are represented by *three upper case characters* whereas end-member components are annotated with *two lower case characters*

Phase	End-member	Component	Formula	Activity relation
PHE	Muscovite	ms	$K(Al)AlSi_2[SiAl]O_{10}(OH)_2$	$Y^2\ (2-Y)$
	Celadonite	ce	$K(Mg)AlSi_2[Si_2]O_{10}(OH)_2$	$0.25\ (1-X_{Fe})\ (1-Y)\ (2-Y)^2$
	Fe-celadonite	fc	$K(Fe)AlSi_2[Si_2]O_{10}(OH)_2$	$0.25\ X_{Fe}\ (1-Y)\ (2-Y)^2$
BIO	Phlogopite	ph	$K\{Mg\}(Mg_2)Si_2[SiAl]O_{10}(OH)_2$	$(1-X_{Fe,M1})^2\ (1-X_{Fe,M2})\ (1-Y)^2\ (1+Y)$
	Eastonite	ea	$K\{Al\}(Mg_2)Si_2[Al_2]O_{10}(OH)_2$	$0.25\ (1-X_{Fe,M2})^2\ (1+Y)^2$
	Annite	an	$K\{Fe\}(Fe_2)Si_2[SiAl]O_{10}(OH)_2$	$X_{Fe,M1}\ X_{Fe,M2}^2\ (1-Y)^2\ (1+Y)$
CHL	Chlinochlore	cl	$Mg_4\{Mg\}(Al)Si_2[AlSi]O_{10}(OH)_8$	$4\ (1-X_{Fe})^5\ (1-Y+N)\ (Y+N)\ (1-Y)\ Y$
	Amesite	am	$Mg_4\{Al\}(Al)Si_2[Al_2]O_{10}(OH)_8$	$(1-X_{Fe})^4\ (Y-N)\ (Y+N)\ Y^2$
	Daphnite	da	$Fe_4\{Fe\}(Al)Si_2[AlSi]O_{10}(OH)_8$	$4\ X_{Fe}^5\ (1-Y+N)\ (Y+N)\ (1-Y)\ Y$
KSP	K-feldspar	or	$KAlSi_3O_8$	No solution considered
QTZ			SiO_2	No solution considered
W			H_2O	No solution considered

Table A1 Thermodynamic data ($\Delta_f H$ is molar enthalpy of formation, SD(H) is the standard deviation on molar enthalpy, S is molar entropy, V is molar volume, a, b, c and d are coefficients in the heat capacity polynomial $C_p = a + bT + cT^{-2} + dT^{-1/2}$, a° is the thermal expansion parameter, κ is the bulk modulus) extracted from THERMOCALC, version 2.5, data set generated 26 September 1997) which was used in calculations presented here. Data for the components ce_{MSz} and fc_{MSz} are from Massonne and Szpurka (1997) and have been converted here into a format consistent with the Holland and Powell data set using PERPLEX (Connolly 1990)

Abbreviation	$\Delta_f H$ (kJ)	SD (H)	S (J° K^{-1})	V (J bar^{-1})	a	b ($\times 10^{-5}$)	c	d	a° (K^{-1})	κ (kbar)
H_2O	−241.81	0.02	188.80	0	0.0401	0.8656	487.5	−0.2512	0.00	0
QTZ	−910.88	0.35	41.50	2.269	0.1107	−0.5189	0	−1.1283	0.65	750
KSP	−3975.1	2.92	216.00	10.892	0.4488	−1.0075	−1007.3	−3.9731	3.35	574
cl	−8929.9	1.85	410.50	21.090	1.1618	1.0133	−7657.3	−9.6909	3.98	472
da	−7154.00	3.33	545.00	21.340	1.2374	1.3594	−3743.0	−11.2500	3.98	472
am	−9052.53	2.02	390.00	20.520	1.1770	0.9041	−7458.7	−10.0530	3.98	472
ph	−6219.44	3.08	328.00	14.964	0.7703	−3.6939	−2328.9	−6.5316	5.79	512
an	−5143.40	3.30	428.00	15.432	0.8157	−3.4861	19.8	−7.4667	5.79	513
ea	−6348.90	4.70	306.00	14.751	0.7855	−3.8031	−2130.3	−6.8937	5.79	513
ms	−5984.10	3.04	292.00	14.083	0.7564	−1.9840	−2170.0	−6.9792	5.96	490
ce	−5844.50	3.04	287.00	14.040	0.7412	−1.8748	−2368.8	−6.6169	5.96	500
fc	−5497.30	3.08	318.00	14.250	0.7563	−1.9147	−1586.1	−6.9287	5.96	490
ce_{MSz}	−5832.42	–	288.53	13.87	0.6459	0.0	−2368.8	−6.6169	5.96	500
fc_{MSz}	−5492.29	–	303.15	13.96	0.6648	0.0	−1246.0	−6.6169	5.96	490

$$CHL + KSP = ms + BIO + QTZ + H_2O + tk\ , \quad (1a)$$

whereas with celadonite as the additive component, the degenerate reaction:

$$ce = KSP + ph + QTZ + H_2O\ , \quad (1b)$$

does not involve chlorite and involves phlogopite (ph). In general, it is useful to choose, for the additive component of a phase exhibiting complex crystalline solution, the end-member component closest to the most abundant naturally occurring compositions. Thus, for biotite, phlogopite (ph) is adequate, and for chlorite, clinochlore (cl). The additive components ms, ph, cl and or are used in Table 1 and in balancing reaction stoichiometries the tk vector is used (Table 2).

2.2 Topology of Tschermak end-member equilibria

In the KFMASH system, there are one divariant equilibrium and six trivariant equilibria involving phengite, chlorite, biotite, K-feldspar, quartz and H_2O. To illustrate the phase diagram topology for this system, it is constructive to select the relevant degenerate phase components and to fix the $Al_2(Fe,Mg)_{-1}Si_{-1}$ and $FeMg_{-1}$ exchanges. This results in the above six phase assemblage stable at an invariant point, and six univariant equilibria, each formed from the invariant assemblage by the absence of one phase (Fig. 1). These equilibria represent limiting cases of the continuous reactions investigated in subsequent sections. The stoichiometric coefficients of the KMASH and KFASH

Table 2 Reaction coefficients, entropy change of reaction (dS_r, J° K^{-1}), volume change of reaction (dV_r, J bar^{-1}) and Clapeyron slope (dP/dT, bar K^{-1}) for various KMASH continuous reactions involving Tschermak exchange (tk, $Al_2Mg_{-1}Si_{-1}$) in muscovite, biotite and chlorite. Reactions are labelled by noting the phase absent (i.e. [phase]) and are written with phases on the high temperature side negative. The compositions of phases are defined in Table 1. The thermodynamic data were calculated at 300 °C, 5kbar. The corresponding water data were calculated using the Holland and Powell (1991, CORK) equation of state. The thermodynamic data for tk were calculated from the relation ce + $Al_2Mg_{-1}Si_{-1}$ = ms. The corresponding KFASH reactions have the same coefficients and similar dS_r, dV_r and dP/dT

Phase absent	Phase components involved in reaction							dS_r (J K^{-1})	dV_r (J bar^{-1})	dP/dT (bar K^{-1})
	ms	ph	cl	or	QTZ	H_2O	tk			
[PHE]	0	−2	1	2	−4	−2	−1	−342.1	1.23	−278
[BIO]	6	0	−1	−6	−2	−2	−5	−440.1	−10.3	43
[CHL]	3	−1	0	−2	−3	−2	−3	−391.1	−4.6	86
[KSP]	3	−3	1	0	−7	−4	−4	−733.2	−3.3	221
[QTZ]	12	2	−3	−14	0	−2	−9	−538.1	−21.9	25
[H_2O]	−3	−1	1	4	−1	0	2	49.0	5.8	8
[tk]	−3	−5	3	8	−9	−4	0	−635.2	8.2	−77

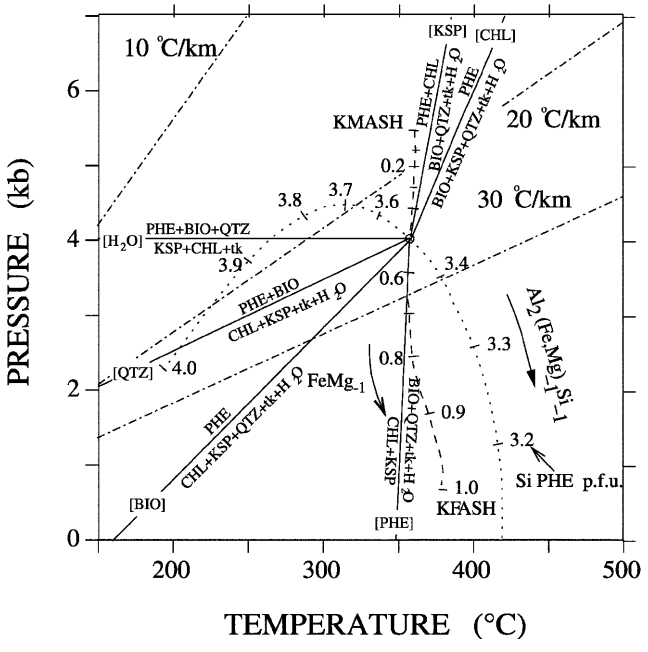

Fig. 1 Calculated topology of reactions emanating from a pseudo-invariant point created by fixing the Tschermak and $FeMg_{-1}$ exchanges (both fixed to 50%) in phengite coexisting with biotite, chlorite, K-feldspar, quartz and water. The *dashed line* shows the displacement locus of the invariant point along the $FeMg_{-1}$ exchange between the end-member invariant points in KMASH and KFASH. The *dotted line* shows variation along Tschermak exchange, $Al_2(Fe,Mg)_{-1}Si_{-1}$ (Si PHE p.f.u. is the silica per formula unit in phengite)

reactions are listed in Table 2. In the remainder of this work, the activities of quartz, K-feldspar and H_2O are taken to be unity.

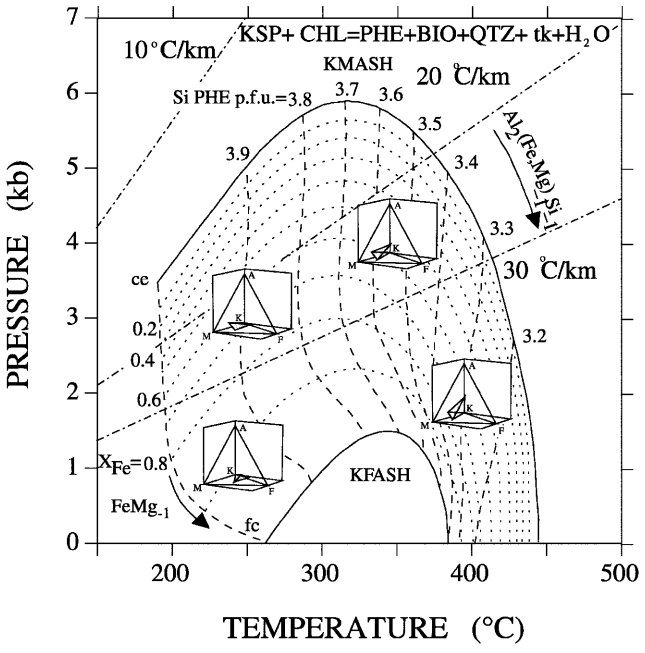

Fig. 2 Calculated *P-T* projection for stability of the assemblage chlorite + K-feldspar (low pressure side) phengite + biotite + quartz + H_2O (high pressure side) in the KFMASH system. The *dashed contours* show the tetrahedral Si (3.2–4) per formula unit (p.f.u.) of phengite in the divariant assemblage, which reflects variations in Tschermak $[Al_2(Fe,Mg)_{-1}Si_{-1}]$ exchange. The *dotted contours* show the X_{Fe} [= Fe/(Fe+Mg)] of phengite in the equilibrium assemblage, and are limited by *solid lines* in the KMASH and KFASH end-member systems. The *inset* Al_2O_3-$KAlO_2$-FeO-MgO (AKFM) tetrahedral phase diagrams (projected from quartz and H_2O) show the calculated compositions of coexisting phengite, biotite, chlorite and K-feldspar at various pressures and temperatures. The linear geothermal gradients (10, 20, 30 °C/km) show that different compositional changes are to be expected during different types of metamorphism

2.3 Stability of the KFMASH divariant assemblage phengite + biotite + chlorite + K-feldspar + quartz + H_2O

In the KFMASH system, the assemblage phengite + biotite + chlorite + K-feldspar + quartz + H_2O is limited by the divariant reaction:

$$\mathrm{CHL + KSP = BIO + PHE + QTZ + tk + FeMg_{-1} + H_2O}\ , \quad (2)$$

whereby the compositions of the coexisting phyllosilicates continuously change with respect to the Tschermak [tk = $Al_2(Fe,Mg)_{-1}Si_{-1}$] and $FeMg_{-1}$ exchanges. The *P-T* projection of this divariant equilibrium can be represented by contouring sets of compositional isopleths for the various phyllosilicate phases. Although we only present compositional isopleths for chemical exchange in phengite (Fig. 2), it is also possible to represent the same phase field by contouring the tk isopleths for biotite and/or chlorite.

Because the $Al_2(Fe,Mg)_{-1}Si_{-1}$ and $FeMg_{-1}$ contents in the coexisting phyllosilicate phases for continuous reactions are strong functions of pressure and tempera-

ture, the stability field of equilibrium (2) extends over a considerable interval of pressure (ca. 6 kbar) and temperature (ca. 250 °C). Although the stability field presented in Fig. 2 delimits the maximum accessible portion of reaction space for equilibrium (2), the effective stability field is likely to be more confined due to the restricted compositional range of natural assemblages. As illustrated by AKFM tetrahedra (inset in Fig. 2), the compositional volume defined by tielines linking the phases phengite-biotite-chlorite-K-feldspar expands with increasing temperature and becomes progressively displaced from Fe- towards more Mg-rich compositions with increasing pressure.

2.4 Stability of KFMASH trivariant assemblages

In the KFMASH system there are six trivariant equilibria involving the phases phengite-biotite-chlorite-K-feldspar-quartz-H_2O (Fig. 1), each of which is formed by the absence of one of the phases from the full assemblage (termed "phase-absent" equilibria, hereafter). Because the calculations were carried out assuming unit activities of both SiO_2 and H_2O, the number of trivariant equilibria considered here reduces to four. In order to present graphically *P-T* projections of the four trivariant KFMASH equilibria, calculations have been performed in the KMASH (Fig. 3a) and KFASH (Fig. 3b) subsystems. This effectively reduces the variance of the assemblage phengite + biotite + chlorite + K-feldspar + quartz + H_2O to univariant, and the phase-absent continuous reactions to divariant. Each phase-absent equilibrium can then be represented by contouring isopleths of the $Al_2(Fe,Mg)_{-1}Si_{-1}$ component, which is directly reflected by variations in the tetrahedral Si content in phengite (Si PHE p.f.u.) and the other phyllosilicate phases. The results of these calculations are presented in Fig. 3a, b.

On the low pressure side of the univariant assemblage phengite + biotite + chlorite + K-feldspar + quartz + H_2O, the two stable divariant equilibria are the phengite-absent assemblage, denoted [PHE] (not shown in Fig. 3), corresponding to the reaction:

$$\mathrm{CHL} + 2\mathrm{KSP} = 2\mathrm{BIO} + 4\mathrm{QTZ} + \mathrm{tk} + 2\mathrm{H_2O}\ , \qquad (3)$$

and the biotite-absent assemblage, denoted [BIO], corresponding to the reaction:

$$6\mathrm{PHE} = \mathrm{CHL} + 6\mathrm{KSP} + 2\mathrm{QTZ} + 5\mathrm{tk} + 2\mathrm{H_2O}\ . \qquad (4)$$

These two assemblages occur in the same *P-T* field but occupy different compositional space, with the biotite-absent equilibria being stable at more Al-rich compositions (see inset AKM diagrams in Fig. 3a). The remaining two divariant equilibria emerge from the high pressure side of the univariant assemblage phengite + biotite + chlorite + K-feldspar + quartz + H_2O. The K-feldspar-absent assemblage, [KSP], which occurs in the more Al-rich compositions, corresponds to the reaction:

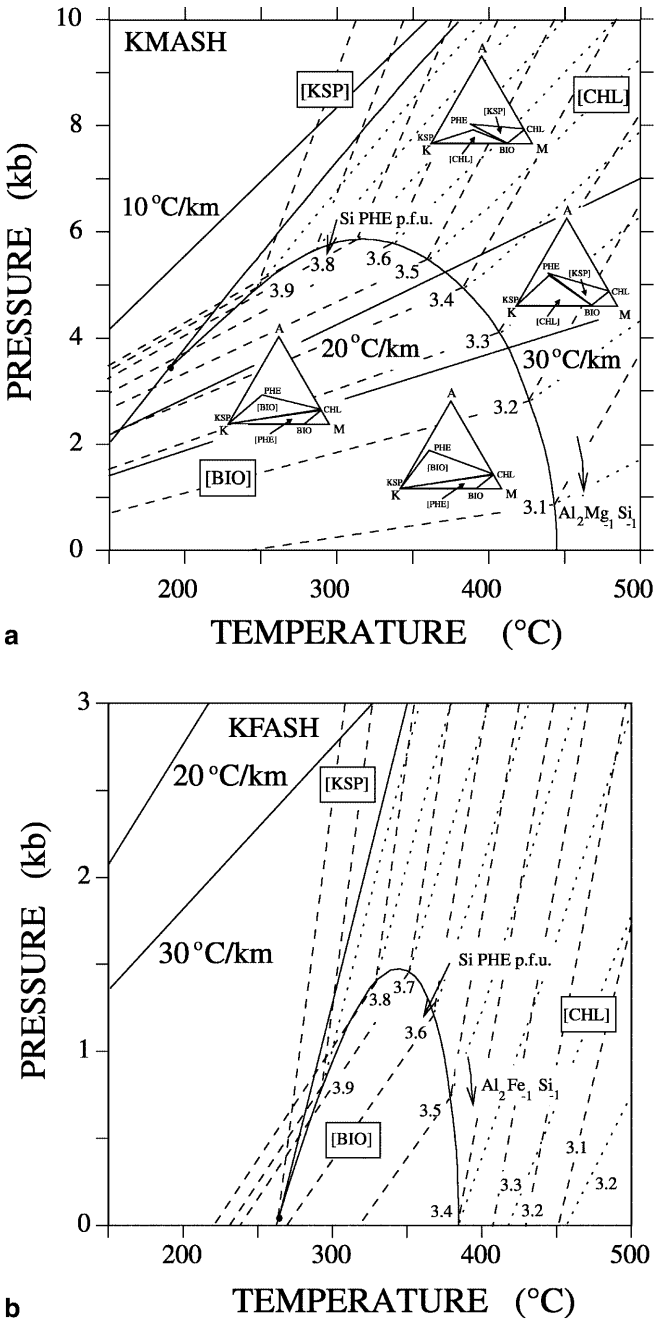

Fig. 3a, b *P-T* projections showing the calculated phase equilibria of assemblages involving phengite, biotite, chlorite, K-feldspar, quartz and H_2O in: **a** KMASH; **b** KFASH (*note different scales*). The phase-absent assemblages, denoted [*phase*], are represented by contouring the tetrahedral silica (Si PHE p.f.u.) of phengite in the various equilibrium assemblages. The *inset* Al_2O_3-$KAlO_2$-MgO (AKM) ternary phase diagrams in **a** (projected from quartz and H_2O) show calculated compositions of the coexisting phases at various pressures and temperatures

$$3\mathrm{PHE} + \mathrm{CHL} = 3\mathrm{BIO} + 7\mathrm{QTZ} + 4\mathrm{tk} + 4\mathrm{H_2O}\ . \qquad (5)$$

The stability of this assemblage has been calculated previously by Powell and Evans (1983) and Bucher-Nurminen (1987) for the KMASH system, and by Roots (1995) in the KFMASH system. The chlorite-absent

assemblage, [CHL], occurs in more Al-poor and K-rich compositions and corresponds to the reaction:

$$3PHE = 2KSP + BIO + 3QTZ + 3tk + 2H_2O \quad . \qquad (6)$$

The stability of this assemblage in the KMASH system has been investigated experimentally by Velde (1965) and Massonne and Schreyer (1987), and has been calculated by Powell and Evans (1983) and Bucher-Nurminen (1987).

3 Continuous equilibria and the construction of *P-T* projections for thermobarometric purposes

We have expanded on previous studies (e.g. Powell and Evans 1983; Bucher-Nurminen 1987) by calculating the full set of continuous equilibria in the KFMASH system (with a variance of 3 or less) existing among the phases biotite, chlorite and K-feldspar (excess quartz and H_2O) which involve phengite. The *P-T* projections of these various equilibria, defined by contouring the $Al_2(Fe,Mg)_{-1}Si_{-1}$ and $FeMg_{-1}$ components in phengite, are presented in Fig. 4. Although isopleths of constant $Al_2(Fe,Mg)_{-1}Si_{-1}$ are only shown in KMASH and KFASH, these isopleths have virtually the same P/T slopes in both chemical systems for fixed $Al_2(Fe,Mg)_{-1}Si_{-1}$. This feature ensures that the isopleths can readily be extrapolated between KMASH and KFASH along contours of constant $Al_2(Fe,Mg)_{-1}Si_{-1}$. Thus, the grids presented in Fig. 4 depict all possible

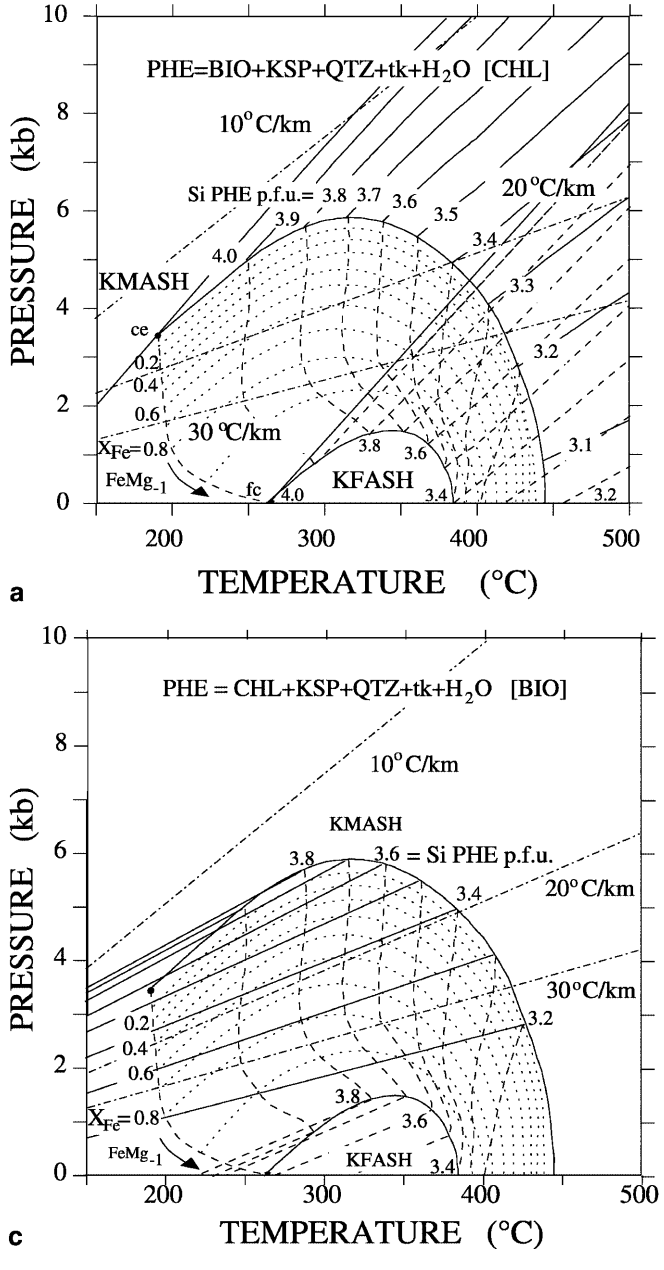

Fig. 4a–c Calculated KFMASH *P-T* projections for the three KFMASH trivariant assemblages existing among K-feldspar, chlorite, biotite involving phengite, quartz and H_2O. The *P-T* projections are contoured in terms of the Tschermak [$Al_2(Fe,Mg)_{-1}Si_{-1}$, represented as Si PHE p.f.u.] and $FeMg_{-1}$ exchanges in phengite. Tschermak isopleths are only shown in the KMASH and KFASH end-member systems. Note that the compositional isopleths have distinctly different slopes for the various buffering assemblages. The potential use of the isopleths as geothermometers or barometers can be assessed from their slope compared to idealised metamorphic paths represented by linear geotherms

compositional variations along $Al_2(Fe,Mg)_{-1}Si_{-1}$ and $FeMg_{-1}$ in phengite within the specified assemblages and they can be used in conjunction with additional mineral compositional data from metamorphic rocks and independent thermobarometric estimates to obtain direct pressure and temperature information.

Although only the phengite composition is needed to construct the trivariant fields presented in Fig. 4, the other phyllosilicate phases have variable compositions which change with phengite. While it is possible to construct equivalent *P-T* grids contouring the $Al_2(Fe,Mg)_{-1}Si_{-1}$ and $FeMg_{-1}$ components in either biotite or chlorite (or both), this possibility is somewhat limited by the more restricted compositional variation exhibited by these phases. As an example, consider the chlorite and biotite compositions coexisting with a phengite composition of $X_{Fe} = 0.11$ and Si p.f.u. 3.12 at a temperature of 260 °C and a pressure of 5 kbar within the assemblage phengite + chlorite + biotite + K-feldspar (+quartz + H_2O) which can be defined (see Table 1) as X(CHL) = 0.013, Y(CHL) = 0.5, N(CHL) = 0.5 and ph(BIO) = 0.92, an(BIO) = 0.002, ea(BIO) = 9×10^{-5}, respectively. Within the same assemblage at 420 °C and 2 kbar the compositions of chlorite and biotite coexisting with a phengite composition of $X_{Fe} = 0.34$ and Si p.f.u. 3.79 are X(CHL) = 0.072, Y(CHL) = 0.504, N(CHL) = 0.496 and ph(BIO) = 0.61, an(BIO) = 0.024, ea(BIO) = 0.067, respectively.

4 Inference of metamorphic histories from continuous reactions

The compositional evolution and mineral zonation recorded during continuous reactions depend on the *P-T* trajectory along which rocks are buried or exhumed. Thus, even though the reactions investigated here have a high variance, they can be used in a classical fashion, similar to low variance reactions, to obtain information on *P-T* paths during a metamorphic episode.

The *P-T* information can be obtained by detailed analysis of the variations in $Al_2(Fe,Mg)_{-1}Si_{-1}$ and $FeMg_1$ contents within rocks of different compositions and within different limiting assemblages. By utilising the fact that the compositional isopleths, defining the various continuous reactions, have different Clapeyron slopes, one can anticipate that the rates and even the signs of chemical exchange may differ for different assemblages undergoing the same metamorphic history. To demonstrate how the metamorphic history may control the compositional trends recorded by continuous reactions, it is useful to consider simple *P-T* trajectories (shown in Figs. 1–3) which correspond to slow burial or exhumation (where heating or cooling keeps pace with pressure changes). The phyllosilicates in rocks of constant Fe^{2+}/Mg buried along low dT/dz gradients (ca. 10 °C/km) will display almost no variation in tk within chlorite-absent assemblages, progressive decreases in tk within K-feldspar-absent assemblages and progressive increases in tk within biotite-absent assemblages (e.g. Fig. 3). In fact within any one limiting assemblage, the trend of compositional variation in $Al_2(Fe,Mg)_{-1}Si_{-1}$ and $FeMg_{-1}$ observed within a profile of exposed rocks may be used to quantify the *T-P* gradient along which rocks were buried or exhumed.

The sequence of reactions observed within rocks of a fixed composition is also sensitively dependent on the *P-T* trajectory of burial or exhumation. Only *P-T* trajectories exceeding approximately 15 °C/km will record the breakdown of chlorite and K-feldspar to form biotite, phengite, quartz and H_2O (reaction 2) with increasing metamorphic grade (Fig. 2). Lower gradients will not experience this reaction but are likely to show the prograde formation of K-feldspar from chlorite at higher metamorphic grades due to the progressive replacement of K-feldspar-absent assemblages by chlorite-absent assemblages (Fig. 3a). This latter reaction is also more likely to be observed in rocks subjected to high *T-P* gradients such as may be observed during periods of isobaric heating.

5 Reaction singularities and the change from hydration to dehydration equilibria

Pressure-temperature curves with maxima (e.g. Fig. 2) indicate that one or more phases have changed sides in a reaction. For each phase changing side in a reaction there is a singularity. As seen from the reaction labelling in Fig. 5, there will be such singularities involving H_2O, QTZ and BIO.

5.1 Reaction singularity reflecting an $Al_2(Fe,Mg)_{-1}Si_{-1}$ degeneracy in phengite

A singularity associated with reaction (2) occurs when phengite is compositionally colinear with chlorite and K-feldspar (solid star in Fig. 5). Close to the degenerate reaction in $KAlO_2$-MgO (ce = ph + KSP + QTZ + H_2O), the phengite composition is less aluminous than the tieline linking coexisting chlorite and K-feldspar and thus phengite undergoes breakdown due to the terminal dehydration reaction:

$$\mathrm{PHE} = \mathrm{CHL} + \mathrm{BIO} + \mathrm{KSP} + \mathrm{QTZ} + \mathrm{tk} + \mathrm{H_2O}\ . \qquad (7)$$

As the $Al_2(Fe,Mg)_{-1}Si_{-1}$ component in the phyllosilicate phases increases, a compositional colinearity is formed among the phases phengite, K-feldspar and chlorite (solid star in Fig. 5) which is represented by the BIO-absent reaction:

$$\mathrm{PHE} = \mathrm{CHL} + \mathrm{KSP} + \mathrm{QTZ} + \mathrm{tk} + \mathrm{H_2O}\ . \qquad (8)$$

At this point, biotite changes side in reaction (2), and the biotite-absent equilibrium emerges tangentially. At higher temperatures, phengite is more aluminous than

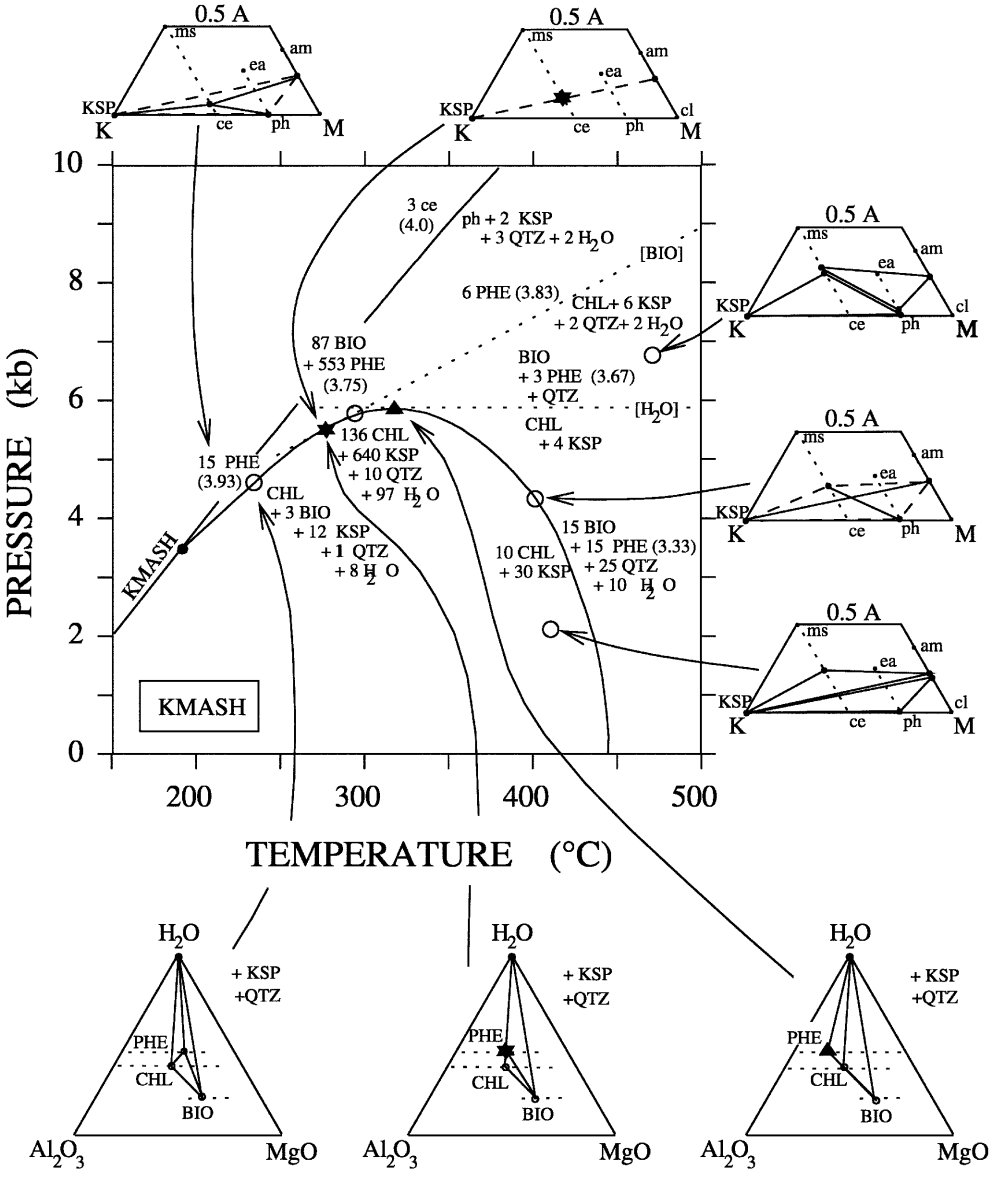

Fig. 5 Calculated KMASH *P-T* projection and schematic ternary (A, Al_2O_3; K, $KAlO_2$; M, MgO) diagrams illustrating phase relations and singularities near the degenerate reaction celadonite → phlogopite + K-feldspar + quartz + H_2O in the $KAlO_2$-MgO system. The *numbers bounded by round brackets* are the calculated tetrahedral Si per formula unit in phengite. The reaction coefficients are obtained using these calculated Si PHE p.f.u. values. In the text these reactions are written more generally involving the tk vector. Singularities which occur in the pressure-temperature space shown are indicated by a *solid star* (biotite-absent reaction) and by a *solid triangle* (H_2O conserving reaction)

the tieline linking chlorite and K-feldspar, so that reaction (2) once again involves biotite with phengite, now in a crossed tieline relationship.

5.2 Singularity involving fluid

As the $Al_2(Fe,Mg)_{-1}Si_{-1}$ component increases further, another compositional colinearity occurs, this time among phengite, biotite and chlorite (with K-feldspar and quartz), which is shown as a solid triangle in projected Al_2O_3-MgO-H_2O diagrams in Fig. 5. At this singularity, H_2O changes side in reaction (2) and a degenerate H_2O-conserving equilibrium emerges tangentially:

$$\mathrm{BIO + PHE + QTZ = CHL + KSP + tk}\ . \qquad (9)$$

At temperatures exceeding that of the singularity, the phengite composition is more aluminous than the tieline linking chlorite and biotite on projected Al_2O_3-MgO-H_2O diagrams. Thus chlorite and K-feldspar break down to form biotite and phengite in the direction of dehydration by the reaction:

$$\mathrm{CHL + KSP = BIO + PHE + QTZ + tk + H_2O}\ . \qquad (10)$$

This appears as a tieline crossing reaction in projected AKM diagrams and as a terminal reaction in projected Al_2O_3-MgO-H_2O diagrams.

The H_2O singularity is located very close to (but not exactly at) the point where the entropy change of reaction (2), and the resulting tangent, go to zero. This property is due to the fact that H_2O is the greatest contributor to the reaction entropy and because the reaction coefficients of H_2O go through zero at the singularity. Unfortunately, the singular behaviour, and the related small entropy changes associated with reaction (2), mean that the location of this phase field (and the

related set of higher variance equilibria) are sensitive to the thermodynamic data set used.

There are several petrological implications related to the presence of the *P-T* maximum of reaction (2). The shallow slope (i.e. dT/dP) of the Tschermak isopleths for the divariant reaction (2) near the maximum (i.e. phengite with Si ca. 3.6 p.f.u.) makes the reaction a potential barometer. In fact, even without mineral compositional data, *maximum* pressure estimates in low grade rocks subjected to relatively high dT/dz conditions can be obtained from reaction (2), and from the two higher variance phase-absent assemblages defined by reactions (3) and (4), which emanate from the low pressure side of reaction (2). More subtle implications resulting from the existence of the *P-T* maximum of reaction (2) are the complex textures and chemical signatures which may result from burial, or exhumation, paths through its phase field. This is particularly important for low-aluminium rocks undergoing burial or exhumation along gradients of approximately 20 °C/km which may show evidence for phengite firstly as a reactant then as a product at different times along the same *P-T* trajectory, for the same rock composition and the same reaction.

6 Petrographic constraints on the mineral stability calculations

To understand how well the thermodynamic calculations in model systems can be applied to natural occurrences for the purposes of thermobarometry, natural examples in which the stability of assemblages involving combinations of the phases phengite, chlorite, biotite, K-feldspar and quartz are constrained by independent thermobarometers have been examined. Table 3 presents a comparison between these independent *P-T* constraints (denoted P_{ref}, T_{ref}), with calculations performed using the data of Holland and Powell (1998) (denoted P_{HP}, T_{HP}) and calculations performed using the data set

Table 3 Comparison between calculated pressures (P_{HP}, P_{MSz}, kbar) and temperatures (T_{HP}, T_{MSz}, °C), pressures estimated on the basis of the Massonne and Schreyer (1987) KMASH isopleths for the chlorite-absent equilibrium (reaction 6, P_{MSc}) and (P_{ref}, T_{ref}) estimates constrained independently from natural data. Phengite compositions are shown in terms of the silica per formula unit (Si p.f.u.) and X_{Fe} [= Fe/Fe + Mg]. The *subscript HP* indicates that the Holland and Powell (1998) phengite data and solution model was used whereas the *subscript MSz* indicates the phengite data and solution model are from Massonne and Szpurka (1997). Calculations were performed with PERPLEX (Connolly 1990) using the data set and solution models of Holland and Powell (1998) and the Holland and Powell (1991, CORK) fluid equation of state. The error bars for P_{HP} (and T_{HP}) are one standard deviation calculated using THERMOCALC. The data presented in the source list below the table indicates the means by which the independent pressure estimates were obtained

Sample	P_{ref} (kbar)	T_{ref} (°C)	Si (p.f.u.)	X_{Fe}	P_{HP}	T_{HP}	P_{MSz}	T_{MSz}	P_{MSc}	Source[a]
Phengite + chlorite + biotite + K-feldspar + quartz										
16	–	–	3.21	0.56	1.3 ± 1.2	409 ± 20	4.3	450	–	17
1407A	–	–	3.17	0.43	1.0 ± 1.2	420 ± 18	2.8	453	–	14
30–44	–	–	3.18	0.47	1.1 ± 1.2	420 ± 20	2.5	443	–	18
33–93	ca. 2	ca. 325	3.19	0.14	0.9 ± 0.8	412 ± 14	2.7	440	–	1
20	–	ca. 450	3.25	0.33	2.6 ± 0.8	412 ± 32	4.1	435	–	4
Phengite + biotite + K-feldspar + quartz [chlorite]										
8/26	>14	500	3.57	0.51	8.5 ± 1.0	–	13.0	–	14.5	11
21	9–14	420–500	3.54	0.69	5.2–7.3 ± 1.0	–	10.0–13.6	–	13.0–14.2	13
M32	6.5	500	3.41	0.49	6.5 ± 1.0	–	10.9	–	14.0	15
WP-9	4.4	720	3.08	0.43	3.2 ± 0.8	–	5.1	–	4.0	7
DDR-14	7–9	600–700	3.29	0.43	7.0–9.1 ± 1.0	–	11.4–15.0	–	9.0–10.0	9
d1	14–15.0	550–600	3.41	0.28	8.5–9.8 ± 1.0	–	10.7–12.5	–	11.5–12.4	12,19
BL-152	ca. 8	ca. 580	3.21	0.35	5.2 ± 1.0	–	7.6	–	7.0	2
PF-114	8.5	575	3.07	0.3	1.3 ± 0.9	–	2.4	–	2.5	3
TC2	9.4	638	3.30	0.45	8.0 ± 1.0	–	13.1	–	10.0	6
Phengite + biotite + chlorite + quartz [K-feldspar]										
12B	6.2	505	3.21	0.45	5.5 ± 1.6	–	8.8	–	–	10
GD80B	7.5	620	3.18	0.31	10.2 ± 1.9	–	15.5	–	–	15
157	3.8	570	3.12	0.46	5.5 ± 1.5	–	9.7	–	–	16
44–93	ca. 2	ca. 535	3.08	0.72	2.1 ± 1.4	–	3.8	–	–	1
TS58	18–22	520–550	3.58	0.02	16.6–18.7 ± 1.8	–	19.7–21.7	–	–	5
2WM3	6.5–7.3	515–530	3.15	0.66	3.6–4.2 ± 1.6	–	8.4–9.5	–	–	8

[a] Sources: (*1* Graessner and Schenk 1999, *2* Rosenberg et al. 1999, sphalerite + pyrrhotite + pyrite barometer, *3* Goscombe et al. 1998, average *PT* calculation, *4* Lentz et al. 1997, *5* Guillot et al. 1997, jadeite + chloritoid + paragonite + garnet and jadeite + garnet + glaucophane + paragonite calculation, *6* DiVincenzo et al. 1997, garnet + plagioclase + muscovite + biotite barometer, *7* Linner 1996, average, *PT* from calculation, *8* Arenas et al. 1995, garnet + plagioclase + muscovite + biotite barometer, *9* Kröner et al. 1995, garnet + hornblende + plagioclase thermobarometer, *10* Bergman 1992, garnet + plagioclase + muscovite + biotite barometer, *11* Massonne and Chopin 1989, presence of jadeite, *12* Mposkos 1989, *13* Evans and Patrick 1987, presence of glaucophane, presence of albite + quartz, *14* Wang et al. 1986, *15* Droop 1985, $jadeite_{ss}$ + quartz + albite and calculation, *16* Novac and Holdaway 1981, calculations using staurolite + silliminite + almandine and staurolite + muscovite + biotite + silliminite, *17* Mather 1970, *18* Ernst 1997, *19* Liati and Mposkos 1990, garnet + pyroxene barometer)

and solution models of Holland and Powell (1998) modified to include the Fe- and Mg-phengite end-member data and solution models of Massonne and Szpurka (1997) (denoted P_{MSz}, T_{MSz}, see Appendix and Table A1). Although the calculations originally presented by Massonne and Szpurka (1997) were carried out using the data set of Berman (1988) augmented by data from a variety of different studies, the Holland and Powell (1998) data were used here in order to focus solely on variations due to the different phengite data and solution models. Table 3 also shows pressure estimates (P_{MS}) based on the isopleths reported by Massonne and Schreyer (1987) for the KMASH chlorite-absent assemblage (reaction 6).

In general, calculations performed with the data of Holland and Powell (1998) yield pressures that are consistent (typically within 2 kbar) with estimations based on independent thermobarometers. There are however some discrepancies, particularly for chlorite-absent assemblages containing high (>40 mol%) celadonite contents (e.g. samples 8/26, 21, d1 in Table 3) where the calculated pressures tend to significantly underestimate the independently derived pressures. One notably anomalous pressure was obtained for a chlorite-absent assemblage in which the calculated pressure estimate is at least 5.0 kbar lower than the pressure indicated from the observed stability of jadeite and quartz at an estimated temperature 500 ± 50 °C (Massonne and Chopin 1989). In fact, the calculated phengite compositional isopleths for the chlorite-absent assemblage have similar *P-T* gradients to the albite + quartz = jadeite isopleths. Assuming the assemblage does represent equilibrium conditions, this relationship implies that either the calculated isopleths at high celadonite content have an incorrect Clapeyron slope or that they are displaced towards too low a pressure. Calculations based on reaction (2) tend to yield realistic temperatures but some unusually low pressures. These anomalous estimates are especially evident for cases in which reaction (2) is described within regional metamorphic terrains (i.e. Scottish Dalradian, Mather 1970; Ryoke metamorphic belt, Wang et al. 1986) where mineral composition data require *T*-z gradients of approximately 60–70 °C/km during burial and prograde metamorphism.

Calculations based on the phengite thermodynamic data and solution model of Massonne and Szpurka (1997) also show a broad agreement with respect to the independent pressure estimates although they also display some discrepancies, most commonly for samples containing phengite with relatively low (<40 mol%) celadonite contents (e.g. samples GD80B, 157, DDR-114, TC2, M32). For such compositions, the calculations generally overestimate the independent pressure estimates (see however sample PF-114). Pressure estimates based on equilibrium (2) are significantly higher than those obtained with the data set of Holland and Powell (1998) and are more consistent with expected *T*-z gradients.

Pressure estimates for the chlorite-absent assemblage based on the isopleths reported by Massonne and Schreyer (1987) are reasonably consistent with independent estimates, with two noticeable exceptions (samples PF-114 and M32) where the differences are between 4 and approximately 6 kbar. Similar discrepancies have been noted by Arenas et al. (1995), Ernst (1997) and Rosenberg et al. (1999). In the latter reference, the difference appears to be due to the application of the Massonne and Schreyer (1987) isopleths for the chlorite-absent assemblage to an assemblage containing coexisting chlorite and K-feldspar (+phengite ± biotite). More recently, Goffé and Bousquet (1997) demonstrated an example in which an entire *P-T* path (spanning 15 kbar and 100 °C) is consistent with a near constant phengite composition existing within different buffering assemblages. These examples outline the inconsistent results that can be obtained by applying phengite barometry to unbuffered assemblages to obtain minimum pressure estimates.

It is difficult to generalise about the relative accuracy of the calculations presented in Table 3 given the limited data available and the uncertain reliability of the independent pressure estimates. However, there does appear to be some tendency for the calculations based on the phengite thermodynamic data set of Holland and Powell (1998) to display greater consistency at relatively low celadonite contents (<40 mol%), whereas the phengite thermodynamic data of Massonne and Szpurka (1997) produce the best results at relatively high celadonite contents (>40 mol%). In all cases, calculations using the Massonne and Szpurka (1997) data can be expected to yield higher pressures than calculations with the Holland and Powell (1998) data. Pressure estimations based directly on the isopleths for the KMASH equilibrium phengite = K-feldspar + biotite + quartz + tk + H_2O experimentally investigated by Massonne and Schreyer (1987) almost always exceed calculation-derived pressures (using thermodynamic data from either Holland and Powell, 1998, or Massonne and Szpurka, 1997).

7 Extension of model calculations to more complex natural systems

Using the Holland and Powell (1998) data set, it is possible to perform internally consistent calculations of a large number of new multivariant reactions involving $Al_2(Fe,Mg)_{-1}Si_{-1}$ in the KMASH, KFASH and KFMASH systems. In the KMASH system, these calculations appear to be accurate for reactions involving phyllosilicates with a high proportion of $Al_2(Fe,Mg)_{-1}Si_{-1}$ exchange (<40 mol% celadonite). The accuracy of calculations involving $Al_2(Fe,Mg)_{-1}Si_{-1}$ exchange in the KFMASH system, and other more complex systems, is less well understood. However, a number of inferences can be made on the basis of petrographic and experimental data.

7.1 Effects due to $FeMg_{-1}$ exchange

Calculations performed with the thermodynamic data set of Holland and Powell (1998) predict that $FeMg_{-1}$ exchange will have a strong influence on the stability of assemblages involving combinations of phengite, chlorite and biotite. The calculated effect of varying $FeMg_{-1}$ on the stability of the various assemblages depends on the $Al_2(Fe,Mg)_{-1}Si_{-1}$ component in the coexisting phyllosilicate phases (Fig. 2). In general, increasing Fe^{2+} relative to Mg^{2+} reduces the pressure at which a particular assemblage is stable. This result contradicts the sparse data available on this subject in two ways. Firstly, mineral exchange data show that the Fe^{2+}/Mg^{2+} ratios of coexisting muscovite and biotite are similar, with the ratios slightly less in phengite than in biotite (Tracy 1978). These data imply that the respective reactions involving phyllosilicate Fe and Mg end-members have similar free energy changes. On the basis of these data, the reaction phengite $\rightarrow$ biotite + K-feldspar + quartz + tk + H_2O should be virtually independent of the Fe^{2+}/Mg^{2+} ratio, not strongly dependent as shown in Fig. 3a, b. Secondly, because the Fe^{2+}/Mg^{2+} ratios are typically slightly less in muscovite than in biotite (Tracy 1978), the addition of Fe^{2+} will actually stabilise biotite + K-feldspar in the chlorite-absent reaction (i.e. reaction 6) and thus reduce the $Al_2(Fe,Mg)_{-1}Si_{-1}$ component in phengite, displacing the Si-isopleths to higher pressure. This is consistent with the experimental data reported by Velde (1965) but contrary to the results of the calculations presented here using the data set of Holland and Powell (1998).

Calculations performed with the phengite end-member data extracted by Massonne and Szpurka (1997) are influenced to a minor extent by the $FeMg_{-1}$ exchange. In general, the effect of increasing Fe^{2+} relative to Mg^{2+} increases the pressure at which a particular assemblage is stable. This behaviour is reflected in results presented in Table 3 where the calculated pressure estimate of sample 21 (13.6 kbar at 500 °C) is greater than that of sample 8/26 (13.0 kbar at 500 °C) the latter of which has a slightly higher celadonite content but significantly lower X_{Fe}. This behaviour is also consistent with the petrographic data outlined above.

7.2 Multi tri- and dioctahedral substitutions

Experimental results and natural data presented by Monier and Robert (1986) demonstrate a complication in addition to that of $FeMg_{-1}$ exchange, in that it was suggested that phengite can deviate significantly from the pure dioctahedral form (e.g. 2Al + vacancy) due to substitution of a trioctahedral (biotite) component (e.g. 3Mg). Based on X-ray diffraction, the trioctahedral component was shown to be important at low temperatures (with an octahedral occupancy of up to 2.2 atoms per formula unit) and to decrease strongly with increasing temperature. Deviations from ideal dioctahedral phengite based on X-ray diffraction were also reported by Massonne and Schreyer (1987) and Massonne and Szpurka (1997) whose data indicate that the octahedral occupancy in phengite increases (relative to 2 p.f.u) with decreasing pressure, and also increases slightly with increasing temperature. Effects due to deviations from dioctahedral phengite are not accounted for in the mixing models and thermodynamic data of Holland and Powell (1998) but are in the data of Massonne and Szpurka (1997). Monier and Robert (1986) indicate that the trioctahedral component in phengite decreases with increasing temperature whereas Massonne and Szpurka (1997) suggest the opposite. The possibility also exists that the trioctahedral component may reflect microscopic phyllosilicate interlayering (e.g. see Garcia-Casco et al. 1993). Its potential importance has been pointed out by Monier and Robert (1986) who suggested that the persistence of the trioctahedral component in phengite to temperatures beyond where there remains significant celadonite component in muscovite may explain the commonly observed presence of octahedrally coordinated divalent cations in phengite at high temperature conditions.

7.3 Effects of additional components, principally Na and Fe^{3+}

Because Na fractionates into K-feldspar more than into coexisting white mica (e.g. Thompson and Thompson 1976) the equilibria investigated here are stabilized by the addition of Na to higher pressures relative to $KAlSi_3O_8$ until saturation with $NaAlSi_3O_8$ occurs. However, because of the limited extent of solid solution between albite and K-feldspar at the conditions of interest in this study, the effect of adding Na is insignificant (calculation showed that the displacement of reaction 2, due to the introduction of Na, was < 100 bar).

Some information also exists on the fractionation of Fe^{3+} and octahedral Al among coexisting phyllosilicates. Mather (1970) presents full chemical analyses for coexisting phengite, chlorite and biotite for reactions across the biotite isograd (reaction 2) in Barrovian series rocks from the Scottish Highlands. The fraction $Fe^{3+}/(Al^{VI} + Fe^{3+})$ is highest in biotite and slightly more in chlorite than phengite (e.g. 0.47, 0.14, 0.13 for sample 11; 0.22, 0.13, 0.07 for sample 16; and 0.22, 0.11, 0.07 for sample 18 of Mather, 1970, p 264). These data indicate that the addition of Fe^{3+} to the systems investigated here will displace reaction 2 towards lower pressure and reactions 5 and 6 towards higher pressure until they saturate with Fe_3O_4 or Fe_2O_3 (or $FeTiO_3$ or TiO_2), depending upon f_{O_2}.

8 Concluding statements

The calculations presented here serve three principal purposes. Firstly, the results constrain the positions of,

and relationships between, various possible phase fields. These reaction topologies provide a quantitative means of understanding the mineralogical changes observed during the metamorphism of natural rocks (Mather 1970; Wang et al. 1986). Secondly, the calculations serve as a means to demonstrate singularities, which are an inherent part of the reactions investigated due to compositional colinearities caused by different amounts of $Al_2(Fe,Mg)_{-1}Si_{-1}$ in the coexisting phyllosilicate phases. A H_2O-absent singularity in particular has petrological significance because it marks the unusual transition from hydration to dehydration associated with a single reaction with increasing pressure and temperature. This behaviour results in a nearly circular phase field (with a maximum in *P-T* space) that provides barometric constraints and may cause complex mineral zonation and chemical signatures in rocks buried or exhumed along *T*-z trajectories exceeding 15 °C/km. Thirdly, the results presented here can be used to obtain quantitative absolute *P-T* estimates and information on the trajectories along which low grade metamorphic rocks are buried and/or exhumed.

The phase relationships, thermobarometric grids and petrological implications that have been discussed in this paper are derived almost entirely on calculations performed with one thermodynamic data set (Holland and Powell 1998). The advantage of this approach is that calculations can be performed within an internally consistent framework. Despite this advantage, we have noted considerable discrepancies between calculations and both petrological and experimental constraints. The calculated pressure differences tend to be small at compositions close to the muscovite end-member (<30 mol% celadonite), but they become increasingly larger as compositions approach the celadonite end-member.

Field and experimental data indicate that calculations overestimate the sign and magnitude of displacements in pressure and temperature induced by the addition of Fe^{2+} to the KMASH system. Given that most experimental data used to derive phyllosilicate data comes from Fe-free systems, thermobarometric calculations are therefore most likely to yield the best results for natural compositions that approach the KMASH system. The trioctahedral substitution [2Al = 3(Fe,Mg), section 7.2] could potentially explain some of the differences between calculations and petrological *P-T* estimations, as could non-ideal octahedral substitutions such as Fe^{3+} for Al. Petrological data indicate the addition of Fe^{3+} to the KMASH system will tend to increase the stability of biotite relative to phengite and chlorite, which will determine whether reactions are displaced towards higher or lower pressure.

Finally, we emphasise that the slope of the isopleths for $Al_2(Fe,Mg)_{-1}Si_{-1}$ are quite different for the various buffering assemblages. In all cases considered here the phases phengite, biotite and chlorite all become less aluminous (more siliceous) with increasing pressure. We encourage determination of mineral compositions in different coexisting assemblages from individual outcrops across metamorphic terrains to determine the effects of Fe^{3+}, Na and Ti on the isopleths presented here.

Acknowledgements This study has benefited from reviews by B.W. Evans, H.-J. Massonne, K.-D. Grevel and R. Powell, from discussions and assistance from B. Worley and from communications with T.J.B. Holland, H.-J. Massonne and K. Bucher-Nurminen. Financial support was provided by ETH-Forschungsprojekt 0-20-885-94.

Appendix: thermodynamic data and comparison of calculations with experimental results

A1 Constraints on stability of the chlorite-absent KMASH assemblage

The only equilibrium considered in this study that has been investigated experimentally is the chlorite-absent assemblage phengite + biotite + K-feldspar + quartz + H_2O (reaction 6). Both Velde (1965) and Massonne and Schreyer (1987) undertook experimental studies of this assemblage in the KMASH system. In both cases, the starting materials were synthetic minerals, oxide mixes or gels. Experimental data extend from 300 to 700 °C, from 2 to 23 kbar and cover phengite compositions ranging from pure muscovite to 80% celadonite. The phengite compositions in both studies were characterised by X-ray powder diffractometry.

The experimental data obtained in the different studies show broadly similar trends (Fig. A1), although the data of Velde (1965) predict greater celadonite contents in phengite at lower pressures and temperatures. Massonne and Schreyer (1987) attributed these differences to the presence of phengite compositions in their experiments that deviated from true dioctahedral compositions and to difficulties encountered by Velde (1965) to satisfy the required conditions of phase characterisation.

Thermodynamic calculations of the KMASH chlorite-absent equilibrium show good agreement with the experimental data for phengite compositions close to the muscovite end-member (<30% celadonite) but show progressively larger deviations as phengite compositions approach the celadonite end-member (Fig. A1). The calculations underestimate the pressure-stability of end-member celadonite by approximately 5 kbar.

A2 Stability of chlorite-absent equilibria based on new data and solution models from Massonne and Szpurka (1997)

Recently, Massonne and Szpurka (1997) have derived new thermodynamic data for the Mg- and Fe-celadonite end-members (Table A1) based on new synthesis experiments involving phengite, garnet, kyanite and quartz or coesite (carried out between 30 and 45 kbar and 850 to 1100 °C), and utilising data from previous experiments carried out by Massonne and Schreyer (1987, 1989). Massonne and Szpurka (1997) also proposed new mixing models to describe the solid solution between Fe- and Mg-celadonite and muscovite. These new models differ from other models (e.g. Holland and Powell, 1990, 1998) in that they are molecular and non-ideal. The non-ideal behaviour of the muscovite-Mg-celadonite solid solution series was modelled by them using an asymmetric Margules formulation, whereas a symmetric model was used for the muscovite-Fe-celadonite solid solution. Exchange between Fe and Mg was assumed to be ideal.

A comparison between phengite isopleths for the chlorite-absent KMASH equilibria presented by Massonne and Szpurka (1997), the corresponding experimental data of Massonne and Schreyer (1987) and calculations performed with the thermodynamic data set of Holland and Powell (1998) is presented in Figs. A1 and A2. Results of calculations (presented by Massonne and Szpurka 1997, their Fig. 7) based on the new data and solution

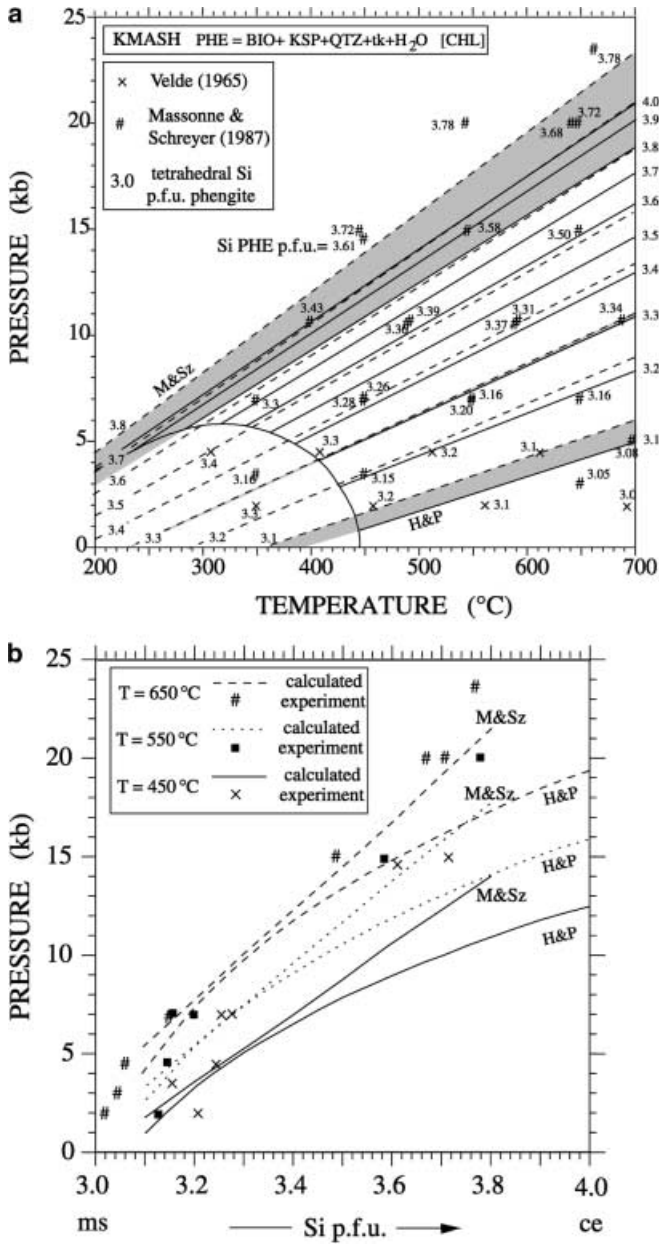

Fig. A1a,b *P-T* projection **a** and *P-X* section **b** showing results of calculations using the thermodynamic data set of Holland and Powell (1998) (*H & P*, *solid lines* in *P-T* projection), isopleths calculated by Massonne and Szpurka (1997) (*M & Sz*, *dashed lines* in *P-T* projection) and experimental data (*P-T* projection: *hash symbols* Massonne and Schreyer 1987, *crosses* Velde 1965, symbols not distinguished in *P-X* section) for the KMASH chlorite-absent assemblage phengite + biotite + K-feldspar + quartz. The *shaded regions* in the *P-T* projection indicate the difference between *H & P* and *M & Sz* calculations for 10, 30 and 80% celadonite

models display a reasonable fit to the experimental data over the entire range of experimentally investigated phengite compositions. The deviation between the two sets of calculations is greatest near to pure celadonite compositions, where the Massonne and Szpurka (1997) isopleths are displaced by approximately 5 kbar towards higher pressure (at constant temperature) relative to isopleths calculated with the Holland and Powell (1998) data set. The deviation between the two sets of isopleths decreases as the muscovite component in phengite increases until 30% celadonite, when the two sets of compositional isopleths nearly coincide. At phengite compositions approaching pure muscovite, the isopleths of Massonne and Szpurka (1997) are displaced by approximately 1 kbar towards higher pressure (at constant temperature) relative to isopleths computed with the Holland and Powell (1998) data set.

A3 Sensitivity of calculations to choice of thermodynamic data and solution models

The results presented in Fig. A1 illustrate that thermobarometric estimations based on the phengite compositions in the chlorite-absent assemblage are dependent on the choice of available thermodynamic data and solution models. These results indicate that it is necessary critically to evaluate the thermodynamic data and solution models prior to applying calculations for thermobarometric purposes.

The difference in thermodynamic data between Holland and Powell (1998) and Massonne and Szpurka (1997) are due to the use of different constraints in the data extraction process. The enthalpy of formation for celadonite was derived by Holland and Powell (1998) from the experiments of Massonne and Schreyer (1989) on the equilibrium talc + muscovite + quartz = celadonite + kyanite + H_2O. These authors pointed out that the resulting data are in reasonable agreement with the experiments of Massonne and Schreyer (1987) and Velde (1965) on the equilibrium celadonite = phlogopite + sanidine + quartz + H_2O, and of Massonne and Schreyer (1987) on the equilibrium muscovite + phlogopite = eastonite + sanidine + quartz + H_2O, but that the results disagree with other experimental results of Massonne and Schreyer (1989). Thermodynamic data for Fe-celadonite were derived by Holland and Powell (1998) using the exchange equilibrium almandine + Mg-celadonite = pyrope + Fe-celadonite investigated by Green and Hellman (1982). Holland and Powell (1998) warned that the errors associated with extracting enthalpy data from exchange equilibria may be considerable because of small free energy and enthalpy changes, especially if one of the phases involved in the exchange is a ternary or higher order solution. Fortunately, THERMOCALC enables the propagation of these uncertainties through the successive calculation which provides an estimation of the resulting thermobarometric errors (see Table 3). For the estimation of entropies, volumes, heat capacities, thermal expansions and compressibilities for celadonite and Fe-celadonite, Holland and Powell (1998) used the experiments of Guggenheim et al. (1987) and Comodi and Zanazzi (1994).

Massonne and Szpurka (1997) derived thermodynamic data for celadonite and Fe-celadonite on the experimental equilibria reported within their 1997 study, along with the data obtained by Massonne and Schreyer (1987, 1989). After estimating molar volumes from the lattice dimensions derived by X-ray diffraction and after introducing Margules parameters to account for the limited miscibility apparent between phengite and phlogopite, enthalpies of formation and entropies were obtained by least squares fitting of results from 48 experiments. The data set of Berman (1988), augmented by data from various other sources, was used as the basis for the thermodynamic evaluation. Recently, Schmidt and Artioli (1999) noted that their new experimental molar volume data for phengite in the KMASH system differ largely from the data of Massonne and Szpurka (1997).

An additional source of variation for calculations presented in Fig. A1 stems from the use of significantly different solution models to describe the mixing in phengite. The variation due to the different solution models is reflected in Fig. A1a by the different spacing between isopleths and in Fig. A2b by the different slopes of the *P-X* curves. Massonne and Szpurka (1997) argue that their data support the deviation from ideal mixing which is interpreted to indicate molecular mixing. They model the non-ideal behaviour using a Margules formulation that is asymmetrical in KMASH and symmetrical in KFASH. These authors demonstrated that such models show a good fit to their experimental data (see also Fig. A1b). Holland and Powell (1998) propose a more classical ionic phengite mixing model in which Mg and Al can only mix on

one (M2A) of two sites and the mixing of tetrahedral Al and Si is restricted to two of the four T sites to maintain Al-avoidance (see also Holland and Powell, 1990). Incidentally the resulting mixing model (and end-member thermodynamic data) shows good agreement with recent experimental data obtained by Schmidt and Artioli (1999).

References

Arenas R, Pascual FJR, Garcia FD (1995) High pressure inclusions and development of an inverted metamorphic gradient in the Santiago-schists (Ordenes complex, NW Iberian Massif, Spain) — evidence of subduction and syncollisional decompression. J Metamorphic Geol 13: 141–164

Bergman S (1992) *P-T*-paths in the Handöl area, central Scandinavia; record of Caledonian accretion of outboard rocks to the Baltoscandian margin. J Metamorphic Geol 10: 265–281

Berman RG (1988) Internally consistent thermodynamic data for minerals in the system Na_2O-K_2O-CaO-MgO-FeO- Fe_2O_3-Al_2O_3-SiO_2- TiO_2-H_2O-CO_2. J Petrol 29: 445–522

Bucher-Nurminen K (1987) A recalibration of the chlorite-biotite-muscovite geobarometer. Contrib Mineral Petrol 96: 519–522

Comodi P, Zanazzi PF (1994) High pressure structural study of muscovite (abstract). In: IMA 16th General Meet, Pisa, pp 79–80

Connolly JAD (1990) Multivariable phase diagrams: an algorithm based on generalized thermodynamics. Am J Sci 290: 666–718

DiVincenzo G, Palmeri R, Talarico F, Andriessen PAM, Ricci CA (1997) Petrology and geochronology of eclogites from the Lanterman Range, Antarctica. J Petrol 38: 1391–1417

Droop GTR (1985) Alpine metamorphism in the south-east Tauern Window, Austria. 1. *P-T* variations in space and time. J Metamorphic Geol 3: 371–402

Ernst WG (1963) Significance of phengitic micas from low-grade schists. Am Mineral 12: 25–62

Ernst WG (1997) Metamorphism of mafic dykes from the central White-Inyo Range, eastern California. Contrib Mineral Petrol 128: 30–44

Essene EJ (1989) The current status of thermobarometry in metamorphic rocks. In: Daly JS, Cliff RA, Yardley BWD (eds) Evolution of metamorphic belts. Geol Soc Spec Publ 43, Oxford, pp 1–44

Evans BW, Patrick BE (1987) Phengite (3T) in high pressure metamorphosed granitic orthogneisses, Seward Peninsula, Alaska. Can Mineral 25: 141–158

Garcia-Casco A, Sanchez-Navas A, Torres-Roldan RL (1993) Disequilibrium decomposition and breakdown of muscovite in high *P-T* gneisses, Betic Alpine Belt (southern Spain). Am Mineral 78: 158–177

Goffé B (1977) Succession de subfacies métamorphiques en Vanoise méridionale (Savoie). Contrib Mineral Petrol 62: 23–41

Goffé B, Bousquet R (1997) Ferrocarpholite, chloritoïde et lawsonite dans les métapélites des unités du Versoyen et du Petit St Bernard (zone valaisanne, Alpes occidentales). Schweiz Mineral Petrogr Mitt 77: 137–147

Goscombe B, Armstrong R, Barton JM (1998) Tectonometamorphic evolution of the Chewore Inliers: partial re-equilibration of high-grade basement during the Pan African Orogeny. J Petrol 39: 1347–1384

Graessner T, Schenk V (1999) Low pressure metamorphism of Palaeozoic pelites in the Aspromonte, southern Calabria: constraints for the thermal evolution in the Calabrian crustal cross section during the Hercynian orogeny. J Metamorphic Geol 17: 157–172

Green TH, Hellman PL (1982) Fe-Mg partitioning between coexisting garnet and phengite at high pressure, and comments on a garnet-phengite geothermometer. Lithos 15: 253–266

Guggenheim S, Chang YH, Koster van Groos AF (1987) Muscovite dehydroxylation: high temperature studies. Am Mineral 72: 537–550

Guidotti CV (1978) Compositional variation of muscovite in medium- to high-grade pelites of northwestern Maine. Am Mineral 63: 878–884

Guidotti CV (1984) Micas in metamorphic rocks. In: Baily SW (ed) Micas. (Reviews in Mineralogy, 13) Mineral Soc Am, Washington, DC, pp 357–467

Guillot S, deSigoyer J, Lardeaux JM (1997) Eclogitic metasediments from the Tso Morari area (Ladakh, Himalaya): evidence for continental subduction during India-Asia convergence. Contrib Mineral Petrol 128: 247–260

Holland TJB, Powell R (1990) An enlarged and updated internally consistent thermodynamic data set with uncertainties and correlations: the system K_2O-Na_2O-CaO-MgO-MnO-FeO- Fe_2O_3-Al_2O_3-TiO_2- SiO_2-C-H_2O-O_2. J Metamorphic Geol 8: 89–124

Holland TJB, Powell R (1991) A compensated – Redlich – Kwong (CORK) equation for volumes and fugacities of CO_2 and H_2O in the range 1 bar to 50 kbar and 100–600 °C. Contrib Mineral Petrol 109: 265–273

Holland TJB, Powell R (1998) An internally consistent thermodynamic data set for phases of petrological interest. J Metamorphic Geol 16: 309–343

Holland TJB, Baker JM, Powell R (1998) Mixing properties and activity-composition relationships of chlorites in the system MgO-FeO-Al_2O_3-SiO_2-H_2O. Eur J Mineral 10: 395–406

Holland TJB, Powell R (1999) Relating formulations of the thermodynamics of mineral solid solutions: activity modelling of pyroxenes, amphiboles and micas. Am Mineral 84: 1–14

James HL (1955) Zones of regional metamorphism in the Precambrian of northern Michigan. Bull Geol Soc Am 66: 1455–1488

Kröner A, Willner AP, Hegner E, Frischbutter A, Hofmann J, Bergner R (1995) Latest Precambriam (Cadomian) zircon ages, Nd isotopic systematics and *P-T* evolution of granitoid orthogneisses of the Erzgebirge, Saxony and Czech Republic. Geol Rundsch 84: 437–456

Lentz DR, Hall DC, Hoy LD (1997) Chemostratigraphic alteration and oxygen isotopic trends in a profile through the stratigraphic sequence hosting the Heath Steele B zone massive sulphide deposit, New Brunswick. Can Mineral 35: 841–874

Liati A, Mposkos E (1990) Evolution of the eclogites in the Rhodope zone of northern Greece. Lithos 25: 89–99

Linner M (1996) Metamorphism and partial melting of paragneisses of the Monotonous Group, SE Moldanubicum (Austria). Mineral Petrol 58: 215–234

Massonne H-J, Chopin C (1989) *P-T* history of the Gran Paradiso (Western Alps) metagranites based on phengite geobarometry. In: Daly JS, Cliff RA, Yardley BWD (eds) Evolution of metamorphic belts. Geol Soc Spec Publ 43, Oxford, pp 545–549

Massonne H-J, Schreyer W (1987) Phengite geobarometry based on the limiting assemblage with K-feldspar, phlogopite, and quartz. Contrib Mineral Petrol 96: 212–224

Massonne H-J, Schreyer W (1989) Stability field of the high pressure assemblage talc + phengite and two new phengite barometers. Eur J Mineral 1: 391–410

Massonne H-J, Szpurka Z (1997) Thermodynamic properties of white micas on the basis of high pressure experiments in the systems K_2O-MgO-Al_2O_3-SiO_2-H_2O and K_2O-FeO-Al_2O_3-SiO_2-H_2O. Lithos 41: 229–250

Mather JD (1970) The biotite isograd and the lower greenschist facies in the Dalradian Rocks of Scotland. J Petrol 11: 253–275

Miyashiro A, Shido F (1985) Tschermak substitution in low- and middle-grade pelitic schists. J Petrol 26: 449–487

Monier G, Robert J-L (1986) Muscovite solid solutions in the system K_2O-MgO-FeO-Al_2O_3-SiO_2-H_2O: an experimental study at 2 kbar P_{H_2O} and comparison with natural Li-free white micas. Mineral Mag 50: 257–266

Mposkos E (1989) High pressure metamorphism in gneisses and pelitic schists in the Eastern Rhodope Zone (N. Greece). Mineral Petrol 41: 337–351

Novac J, Holdaway MJ (1981) Metamorphic petrology, mineral equilibria and polymetamorphism in the Augusta quadrangle, south-central Maine. Am Mineral 66: 51–69

Powell R, Evans JA (1983) A new geobarometer for the assemblage biotite- muscovite-chlorite-quartz. J Metamorphic Geol 1: 331–336

Powell R, Holland TJB (1988) An internally consistent data set with uncertainties and correlations. 3. Applications to geobarometry, worked examples and a computer program. J Metamorphic Geol 6: 173–204

Powell R, Holland TJB (1990) Calculated mineral equilibria in the pelite system, KFMASH (K_2O-FeO-MgO-Al_2O_3-SiO_2-H_2O). Am Mineral 75: 367–380

Powell R, Holland TJB, Worley B (1998) Calculating phase diagrams involving solid solutions via non-linear equations, with examples using THERMOCALC. J Metamorphic Geol 16: 577–588

Roots M (1995) Tschermak substitution in the assemblage muscovite-biotite-chlorite-quartz; a comparison between natural and thermodynamic data. Neues Jahrb Mineral Monatsh 2: 75–95

Rosenberg JL, Spry PG, Jacobson CE, Cook NJ, Vokes FM (1999) Thermobarometry of the Bleikvassli Zn-Pb(-Cu) deposit, Nordland, Norway. Miner Deposita 34: 19–34

Sassi FP (1972) The petrological and geological significance of the b_o values of potassic white micas in low-grade metamorphic rocks. An application to the Eastern Alps. Tschermaks Mineral Petrogr Mitt 18: 105–113

Schmidt MW, Artioli G (1999) Molar volumes of the phengite solid solution in KMASH (K_2O-MgO-Al_2O_3-SiO_2-H_2O) and consequences on geobarometry (abstract). Conf Abstr 4: 708

Spear FS (1989) Relative thermobarometry in metamorphic rocks. In: Daly JS, Cliff RA, Yardley BWD (eds) Evolution of metamorphic belts, Geol Soc Spec Publ 43, Oxford, pp 63–81

Thompson JB, Thompson AB (1976) A model system for mineral facies in pelitic schists. Contrib Mineral Petrol 58: 243–277

Thompson AB (1976) Mineral reactions in pelitic rocks. I. Prediction of *P-T-X*(Fe-Mg) phase relations. Am J Sci 276: 401–424

Thompson AB (1982) Dehydration melting of pelitic rocks and the generation of H_2O-undersaturated liquids. Am J Sci 282: 1567–1595

Thompson JB (1957) The graphical analysis of mineral assemblages in pelitic schists. Am Mineral 42: 842–858

Thompson JB (1979) The Tschermak substitution and reactions in pelitic schists (in Russian). In: Zharikov VA, Fonarev WI, Korikovsii SP (eds) Problems in physicochemical petrology, Vol Korzhinskii DS. Moscow Acad Sci, pp 146–159

Tracy RJ (1978) High-grade metamorphic reactions and partial melting in pelitic schist, West-Central Massachusetts. Am J Sci 278: 150–178

Velde B (1965) Phengite micas: synthesis, stability and natural occurrence. Am J Sci 263: 886–913

Wang GF, Banno S, Takeuchi K (1986) Reactions to define the biotite isograd in the Ryoke metamorphic belt, Kii Peninsula, Japan. Contrib Mineral Petrol 93: 9–17

Worley B, Powell R (1998) Singularities in NCKFMASH (Na_2O-CaO-K_2O-MgO-FeO-Al_2O_3-SiO_2-H_2O). J Metamorphic Geol 16: 169–188

Zen E-an (1960) Metamorphism of Lower Palaeozoic rocks in the vicinity of the Taconic Range in west-central Vermont. Am Mineral 45: 129–175